D.I. ZHUKHOVITSKII,[1] V.E. FORTOV,[1] V.I. MOLOTKOV,[1] A.M. LIPAEV,[1]
V.N. NAUMKIN,[1] H.M. THOMAS,[2] A.V. IVLEV,[2] G.E. MORFILL[2]

[1] Joint Institute of High Temperatures, Russian Academy of Sciences
(Bd. 2, 13, Izhorskaya Str., Moscow 125412, Russia; e-mail: dmr@ihed.ras.ru)
[2] Max-Planck-Institut für Extraterrestrische Physik
(Giessenbachstrasse, 85748 Garching, Germany)

SUBSONIC MOTION OF A PROJECTILE IN A FLUID COMPLEX PLASMA UNDER MICROGRAVITY CONDITIONS

UDC 533.92

Subsonic motion of a large particle moving through the bulk of a dust crystal formed by negatively charged small particles is investigated, by using the PK-3 Plus laboratory on the board of the International Space Station. Tracing the particle trajectories shows that the large particle moves almost freely through the bulk of a plasma crystal, while dust particles move along characteristic α-shaped pathways near the large particle. We develop a theory of the nonviscous motion of dust particles near a large particle and calculate particle trajectories. The deformation of a cavity around a large projectile moving with subsonic velocity in the cloud of small dust particles is investigated with a due regard for the friction between dust particles and atoms of a neutral gas. The pressure of a dust cloud at the surface of a cavity around the projectile can become negative, which entails the emergence of a considerable asymmetry of the cavity, i.e., the cavity deformation. The corresponding threshold velocity is calculated, which is found to decrease with increasing the cavity size. A good agreement with experiment validates our approach.

Keywords: dusty plasma, plasma crystal, nonviscous motion, cavity deformation.

1. Introduction

Complex (dusty) plasma is a low-temperature plasma including microparticles. Due to the electron absorption, particles acquire a considerable electric charge. Thus, a strongly coupled Coulomb system is formed [1–9]. Such plasma represents a natural system, which makes it possible to observe various collective phenomena at the level of individual particles. In experimental setups, complex plasmas are usually studied in gas discharges at low pressures, e.g., in radio frequency (RF) discharges. A large homogeneous bulk of complex plasma, which almost fills the entire discharge volume, can be observed under microgravity conditions either in parabolic flights [10–14] or on the board of the International Space Station (ISS) [10, 15–19].

In recent studies, the attention was focused on tracer particles or projectiles moving through a cloud of complex plasma. Such projectiles are generated using controlled mechanisms of acceleration [11, 20], or they can appear sporadically [19, 21]. Projectiles moving with supersonic velocity lead to the formation of extended Mach cones; subsonic (slow) ones produce localized disturbances of surrounding particles. In Ref. 22, it was suggested that the latter regime, realized when a relatively large subsonic projectile moves in a dense cloud of smaller particles, can be well approximated by a flow of an incompressible fluid. In the framework of the same hydrodynamic approximation, it was demonstrated that, along with the regular neutral gas drag, there is an additional force exerted on the projectile due to the friction between neutral atoms and the particle fluid [25].

Using the PK-3 Plus laboratory on the board of the ISS, we have investigated the motion of dust particles in a vicinity of the moving large particle. Such relatively slow particles are accelerated spontaneously on the outside of the particle cloud in an RF discharge, penetrate into the dust cloud, and move inside it. We have made a series of snapshots of this motion in the plane of a laser sheet with a high-resolution camera, which allowed us to trace the trajectories of individual

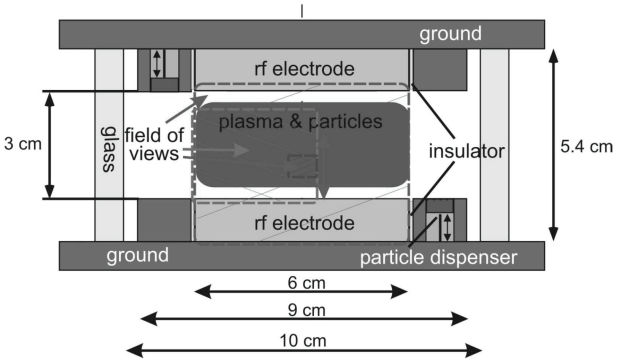

Fig. 1. (Color online) The cross-sectional schematic of a plasma chamber

particles. Motion of small particles caused by the passage of a large particle has already been studied and used as a source of valuable information in the course of a ground-based experiment [24], where heavy particles were dropped down to the cloud of dust particles levitating in the plasma sheath region of a RF capacitive planar discharge. Trajectories of particles suspended in low-pressure glow discharges have also been studied in [20]. Dust particles were arranged in chains, and a heavy particle falling between neighboring dust chain bundles caused the elliptic motions of the background dust particles.

A superposition of successive frames recorded in our experiment reveals that many more dust particles in a close neighborhood of a moving particle circumscribe typical α-shaped trajectories, while other particles remain almost at rest. We interpret this motion as a nonviscous flow about a large particle, for which we used the hydrodynamic approach. Based on the classical solution of the Navier–Stokes equation for the velocity field, we integrate it to obtain streamline pathways for individual dust particles. A good agreement between recorded and calculated trajectories validates our basic assumption.

In this study, we try to estimate the deformation threshold for an (initially spherical) cavity around a subsonic projectile. This deformation emerges abruptly as the projectile velocity increases, as it is seen in snapshots given in [11, 22]. To solve this problem, we employ the Navier–Stokes equation for a compressible fluid with regard for the friction between dust particles and atoms of a neutral gas. We do not treat the deformation self-consistently. Instead, we imply that the projectile velocity is below the threshold value, so that a regular flow around a spherical cavity with no stall can be treated. The solution shows that, due to the friction, the pressure of a dust cloud at the boundary of the cavity behind the projectile can become negative, which entails the formation of a microscopic void free from dust particles, i.e., the cavity deformation. This occurs at some threshold velocity, which decreases with increasing the cavity size. The measurement of such velocity would make it possible to estimate the static pressure inside the dust cloud.

The paper is organized as follows. In Section 2, we describe the experimental setup and the results of tracing the dust particle motion caused by the passage of a large particle. In Section 3, we solve the Navier–Stokes equation for an incompressible particle fluid and obtain both numerical and analytical solutions for dust particle trajectories. In Section 4, the gas dynamics problem is solved, and the corrections due to the fluid compressibility to the velocity and pressure fields are calculated. The calculation results are compared with available experimental data in Section 5, and the results of this study are summarized in Section 6.

2. Experimental Setup and Results

Here, we present an observation of the subsonic nonviscous motion of a large particle in the bulk of a three-dimensional complex plasma in the PK-3 Plus laboratory on the board of the ISS. Details on the setup can be found in [18]. The heart of this laboratory consists of a capacitively coupled plasma chamber with circular electrodes of 6 cm in diameter and 3 cm apart (see Fig. 1).

Microparticles can be injected into the main plasma with dispensers. The particles form then a cloud around the center of the chamber, typically with a central void caused by the ions streaming outward. Generally, some larger particles are present in the chamber as well. The origin of these particles is not yet understood; these might be, for instance, agglomerates or larger particles left over from previous experiments (not removed during the cleaning procedure). They normally accumulate themselves at the periphery of the particle cloud, because of the dependence of the ratio of the electric and ion drag forces on the particle diameter [25]. Sometimes, one of these larger particles gets sporadically accelerated

and penetrates into the cloud – we shall call it a projectile. The reason for such behavior remains a puzzle (e.g., it might be caused by a laser-induced rocket force [26]). Nevertheless, these particles can be used as natural probes of the microparticle cloud [27, 28] in the same way as particles injected on purpose [10, 14, 29]. Projectiles enable various active experiments to be performed in a wide range of testing parameters, thus providing the opportunity to reveal new features of strongly coupled complex plasmas. In particular, the velocities of projectiles can vary significantly, and when they move through a cloud of background microparticles at supersonic velocities, they excite Mach cones [19]. On the other hand, the obvious disadvantage of experiments with projectiles is that their velocities cannot be controlled.

In what follows, we discuss, in detail, one example of a slow (subsonic) motion of a projectile. The experiment was performed during the 13th mission of PK-3 Plus on the ISS. Argon was used as a buffer gas at a pressure of 10 Pa, and the main microparticle cloud was composed of melamine-formaldehyde particles 2.55 μm in diameter. The projectile was accelerated from the side and penetrated into the main cloud, moving almost horizontally from the left to the right (see Fig. 2, *a*, phase I).

To determine the size of the projectile, this experiment was compared with others performed with larger particles, which allowed us to conclude that the projectile radius was $a_p = 7.5$ μm. During its path toward the void, the velocity of the projectile varied, decreasing from 80 mm/s to 37 mm/s. Inside the void, the horizontal motion further slowed down. The particle was then accelerated upward (see Fig. 2, *a*, phase II), where it again penetrated into the microparticle cloud (see the discussion of microparticle trajectories in Ref. [19]). In the region above the void, the particle was slower than before. It did, however, push the microparticles away to clear its path. Figure 2, *b* shows the projectile motion during phase II. The microparticles that were pushed away moved in vortices around the probe particle. The projectile accelerated while traveling upward through the microparticle cloud, so that its velocity increased from 7 to 14 mm/s. This value is still lower than the speed of sound.

In the experiments, we monitored the motion of dust particles in a vicinity of the projectile, by manually determining its position recorded by a high-

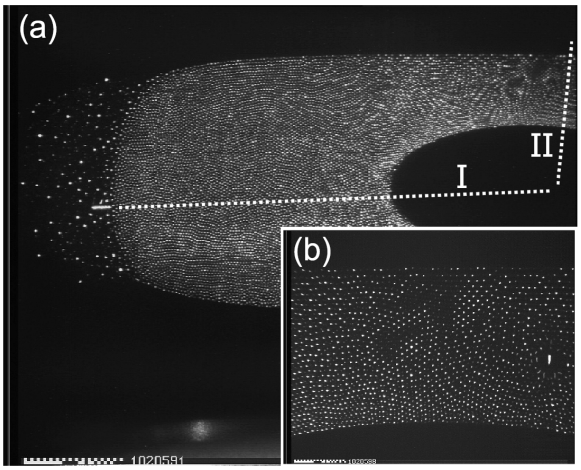

Fig. 2. (*a*), snapshot of the microparticle cloud from quadrant view camera (field of view is 35.7 mm × 26.0 mm). On the left-hand side, a small track of the initial movement of a probe particle (projectile) into the cloud is visible. The horizontal dashed line shows schematically the path of the projectile on the left-hand side (phase I); the vertical dashed line is the path of projectile from the void into the upper part of the microparticle cloud (phase II). (*b*), snapshot of the microparticle cloud from a high-resolution view camera (field of view is 8.1 mm × 5.9 mm). A small track on the right-hand side shows the projectile motion in phase II

resolution camera at 50 frames/s (a video frame is illustrated in Fig. 2, *b*). The horizontal and vertical resolutions of the camera were 11.3 and 10.3 μm per pixel, respectively.

The projectile motion from the void to the chamber wall is represented by frames from bottom to top in Fig. 3.

Dust particles form a dust crystal, which can be represented as a set of Wigner–Seitz cells around each particle. We estimate the dust particle number density as $n_\mathrm{d} = 3 \times 10^5$ cm^{-3}; hence, the cell radius is $\bar{r}_\mathrm{d} = (3/4\pi n_d)^{1/3} = 9.3 \times 10^{-3}$ cm. We can define the coupling parameter of the interaction between the projectile and dust particles (or the scattering parameter) $\beta_\mathrm{dp} = 2Z_\mathrm{p}Z_\mathrm{d}e^2/\lambda M_d u^2$ as the ratio of the characteristic Coulomb energy $Z_\mathrm{p}Z_\mathrm{d}e^2/\lambda$ at the plasma (ion) screening length λ (where Z_p and Z_d are the charges of the projectile and a dust particle, respectively, in units of the electron charge e) to the kinetic energy of a dust particle $M_\mathrm{d}u^2/2$ in the reference frame co-moving with the projectile (where $M_\mathrm{d} = 1.31 \times 10^{-11}$ g is the dust particle mass, and $u \simeq 1$ cm/s is the projectile velocity). Based

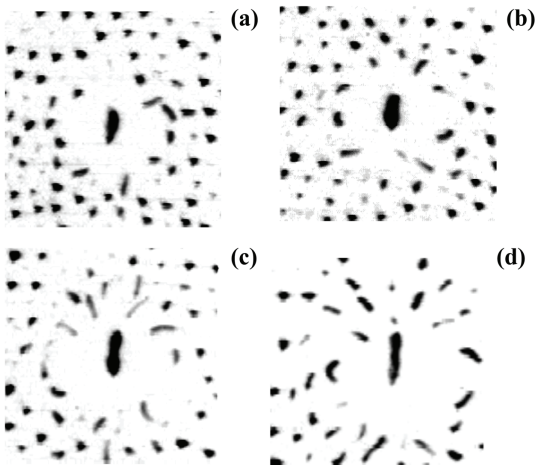

Fig. 3. Positions of dust particles and the projectile (negative images) at successive instants. Time interval between individual frames is 0.08 s. Frames (*a*) and (*b*) illustrate a spherical cavity; (*c*) and (*d*), deformed cavity. The projectile is accelerated from (*a*) to (*d*)

on the analysis of recent melting experiments performed under identical conditions [17], we estimate $\lambda \simeq 6 \times 10^{-3}$ cm, $Z_{\rm d} \simeq -1200$ and, assuming a linear scaling of the charge with size, $Z_{\rm p} \simeq -7000$. This yields $\beta_{\rm dp} \simeq 100$. Hence, the estimate for the radius of the strong interaction between the projectile and dust particles gives [6] $\simeq \lambda \ln \beta_{\rm dp} \simeq 2.7 \times 10^{-2}$ cm. This value turns out to be fairly close to the average distance between the projectile and nearest dust particle neighbors, $R \simeq 3.74 \times 10^{-2}$ cm. The superposition of frames like those shown in Fig. 3 reveals trajectories of individual dust particles that move along loops of similar form (Section 3). It is also seen that the projectile is surrounded by a cavity. The projectile is first centered in a cavity, and then it is shifted toward its front edge (Section 5).

3. Nonviscous Dust Particle Motion in the Incompressible Fluid Approximation

Consider the irrotational flow of an incompressible particle fluid formed by the dust crystal melted around a projectile moving with the velocity $\mathbf{u}(t)$ relative to the dust, where t is the time. The Navier–Stokes equation describing the velocity field $\mathbf{v}(\mathbf{r}, t)$ in the reference frame of the projectile has the form

$$\frac{\partial \mathbf{v}}{\partial t} + (\mathbf{v} \cdot \nabla)\mathbf{v} + \nu(\mathbf{v} + \mathbf{u}) = -\frac{\nabla p}{\rho}, \qquad (1)$$

where $\rho = M_{\rm d} n_{\rm d}$ is the mass density of the dust fluid (assumed in this section to be constant), with M_d and n_d being, respectively, the mass and the number density of dust particles of the radius $a_{\rm d}$. Furthermore, $p(t, \mathbf{r})$ is the dust pressure field, $\nu = (8\sqrt{2\pi}/3)\delta m_n n_n v_{Tn} a_{\rm d}^2 / M_{\rm d}$ is the friction coefficient with $\delta \simeq 1.4$ being the accommodation coefficient [6], and m_n, n_n, T_n, and $v_{Tn} = (T_n/m_n)^{1/2}$ are the mass, number density, temperature, and thermal velocity of neutral gas molecules, respectively. Equation (1) assumes also that, far from the projectile, dust particles are quiescent relative to the neutral gas. It was shown in [22] that the approximation of nonviscous flow results in a fairly good description of trajectories of individual dust particles; the estimate of the viscosity term for the dust particle fluid is indicative of the fact that, in most cases, it is small [23]. This allowed us to omit it in Eq. (1) and to confine ourselves to the nonviscous approximation.

For an incompressible fluid, the continuity equation is reduced to

$$\nabla \cdot \mathbf{v} = 0. \qquad (2)$$

The boundary conditions for (1) and (2) are $(\mathbf{v} \cdot \mathbf{n})|_{r=R} = 0$, where $\mathbf{n} = \mathbf{r}/r$, and $\mathbf{v} = -\mathbf{u}$ at $r = \infty$. For an irrotational flow ($\nabla \times \mathbf{v} = 0$), we substitute $\mathbf{v} = \nabla\varphi - \mathbf{u}$ in Eq. (2) to obtain the equation

$$\nabla^2 \varphi = 0, \quad \varphi(t, \infty) = 0, \quad \left.\frac{\partial \varphi}{\partial \mathbf{n}}\right|_{r=R} = 0, \qquad (3)$$

which has the solution [30]

$$\varphi(\mathbf{r}) = -\frac{R^3}{2r^2}\mathbf{u} \cdot \mathbf{n} \qquad (4)$$

or

$$\mathbf{v}(\mathbf{r}) = -\frac{R^3}{2r^3}\left[\mathbf{u} - 3\mathbf{n}(\mathbf{n} \cdot \mathbf{u})\right] - \mathbf{u}. \qquad (5)$$

The streamlines can be obtained by integration of Eq. (5) in the laboratory reference frame. Let the X-axis be directed along the motion of a sphere. Then the vector $\mathbf{n}$ has the components $\{(x - ut)/r,\ y/r,\ z/r\}$, where $r = [(x - ut)^2 + y^2 + z^2]^{1/2}$ and $\mathbf{u} \cdot \mathbf{n} = (x - ut)u/r$. We introduce the variables $\zeta = (x - ut)/R$, $\eta = y/R$, and $\tau = \nu t$, where $\nu = 3u/2R$, to rewrite Eq. (5) as a system of differential equations,

$$\begin{aligned} \frac{d\zeta}{d\tau} &= \left(\frac{\zeta^2}{\zeta^2 + \eta^2} - \frac{1}{3}\right)\left(\zeta^2 + \eta^2\right)^{-3/2} - \frac{2}{3}, \\ \frac{d\eta}{d\tau} &= \zeta\eta\left(\zeta^2 + \eta^2\right)^{-5/2}, \end{aligned} \qquad (6)$$

with the initial conditions $\zeta(0) = 0$ and $\eta(0) = \eta_0$ ($|\eta_0| \geq 1$). Due to the axial symmetry, the third equation for Z-axis coincides with the second equation in (6) and is therefore redundant.

Because a decrease of the particle velocity (5) with the distance from the projectile is rather fast, $|\mathbf{v}| \propto \propto r^{-3}$, we can assume that particles move in a thin fluid tube in a vicinity of the sphere with the radius R so that the difference between r and R can be neglected, and $\zeta^2 + \eta^2 \simeq 1$. Equations (6) are then reduced to

$$\begin{aligned} \frac{d\zeta}{d\tau} &= \zeta^2 - 1, \\ \frac{d\eta}{d\tau} &= \zeta\eta, \end{aligned} \tag{7}$$

with the initial conditions $\zeta(0) = 0$ and $\eta(0) = 1$. Within the framework of this approximation, we have to assume also that a particle is quiescent until it finds itself on the surface of the moving sphere (projectile cell). This instant corresponds to the time $t = -\Delta t$ and to the distance d between the particle and the projectile motion direction (impact parameter). Obviously, the solution of Eqs. (6) obeys the condition $|\eta(\pm\infty)| = d/R$. Due to the time reversibility of Eqs. (7), the particle must stop at $t = \Delta t$ and further remain quiescent, the total time of motion being $2\Delta t$. Thus, the initial conditions should be completed by the "collision" condition $\eta(\Delta t) = \pm d/R$, where the sign of d defines the particle motion direction. We integrate Eqs. (7) to derive $\zeta(\tau) = -\tanh\tau$ and $\eta(\tau) = (\cosh\tau)^{-1}$. In conventional units, we obtain [22]

$$\begin{aligned} x^* &= \frac{x}{R} = \frac{2}{3}\nu t - \tanh\nu t, \\ y^* &= \frac{y}{R} = \frac{1}{\cosh\nu t}. \end{aligned} \tag{8}$$

From the second equation in (8), we obtain

$$\Delta t = \nu^{-1} \ln\left(\frac{R}{d} + \sqrt{\frac{R^2}{d^2} - 1}\right). \tag{9}$$

If $1 - (d/R) \ll 1$, we find approximately $\Delta t \simeq \simeq (2R/d - 2)^{1/2}$ for a grazing collision. At $(d/R) \ll \ll 1$, we have $\Delta t \simeq \ln(2R/d)$. It was shown in Ref. [22] that the approximate solution almost coincides with the numerical solution of the system of equations (6) corresponding to the same d/R. Our approximation is valid even at a large impact parameter $d = R$, because the numerical solution of (6) yields $y(0) = 1.33R$ in this case, i.e., the distance between the particle and the projectile is still not much different from R.

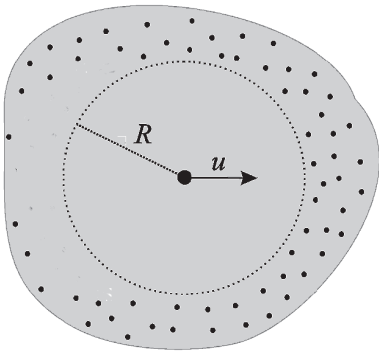

Fig. 4. Deformation of a cavity behind the moving projectile (large bullet in the center) moving with the velocity u through the dust crystal (small bullets around) in a carrier gas. The projectile is surrounded by a deformed cavity with initial radius R

The pressure field $p(\mathbf{r})$ can then be found by substituting velocity (5) in Eq. (1). This yields the following pressure distribution at the spherical surface of a cavity ($r = R$),

$$p = p_{\rm st} + \frac{\rho\nu R}{2}\mathbf{u}\cdot\mathbf{n} + \frac{\rho u^2}{8}\left[9\frac{(\mathbf{u}\cdot\mathbf{n})^2}{u^2} - 5\right] + \frac{\rho R}{2}\dot{\mathbf{u}}\cdot\mathbf{n}, \tag{10}$$

where $p_{\rm st} = \text{const} > 0$ is the static pressure of dust at $r = \infty$.

It can be shown that, along with the regular neutral gas drag, there is an additional force exerted on the projectile due to the dissipation in the surrounding particle fluid. This force can be calculated using the pressure distribution (10). Thus, we have [23]

$$F_{\rm d} = 2\pi R^2 \int\limits_{-1}^{1} \xi p(R, \xi)\, d\xi = -\frac{2\pi}{3} m_{\rm d} n_{\rm d} R^3 \nu u, \tag{11}$$

where $m_{\rm d}$ is the dust particle mass. This additional force can provide a significant contribution to the total drag.

Consider the deformation of a cavity around the projectile propagating in the dust crystal (Fig. 4).

Here, we will neglect the finite fluid compressibility – corresponding corrections are discussed in Section 4. Deformation can be caused solely by the formation of a void in the dust fluid stream, because the interaction parameter β_{dp} is large. Since no evidence for an appreciable attraction between dust particles has been reported in the literature, we model the cloud of dust particles by a system of hard spheres. In such a system, a cavity can be deformed by the void formation if the condition $p \leq 0$ is satisfied over some area around a cavity. This condition corresponds to the cavitation in a metastable fluid and to a stall in the gas dynamics.

Let us first consider the case $\dot{u} = 0$. According to Eq. (10), the friction between dust particles and the neutral gas gives rise to an increase in the pressure in front of the projectile and a decrease behind it, so that $p(\mathbf{r})$ reaches a maximum at the "front pole" (where $\mathbf{u} \cdot \mathbf{n} = u$). By introducing the cosine of the polar angle, $\cos\theta = \mathbf{u} \cdot \mathbf{n}/u \equiv \xi$, we readily derive

$$\frac{\partial p}{\partial \xi} = \frac{9}{4}\rho u^2(\xi - \xi_{\rm cr}), \tag{12}$$

where $\xi_{\rm cr} = -2\nu R/9u$. If $|\xi_{\rm cr}| > 1$, then the pressure reaches a minimum at the "rear pole" ($\xi = -1$), where $p_{\min} = p_{\rm st} - \rho u^2(9|\xi_{\rm cr}|/2 - 1)/2$. This corresponds to the low-velocity regime $u < 2\nu R/9$, when the minimum pressure decreases (approximately) linearly both with u and R. The cavity deformation threshold is defined by the condition $p_{\min} = 0$ and is reached easier for larger projectiles, at the critical velocity $u_{\rm cr} \simeq 2p_{\rm st}/(\rho\nu R)$ [here, we assume $p_{\rm st} \lesssim \rho(\nu R)^2/8$]. Note that, in the high-velocity regime $u > 2\nu R/9$, the pressure minimum is shifted to a certain latitude in the rear hemisphere, approaching the "equator" ($\xi = 0$) asymptotically. In this case, the friction plays a minor role, and the critical velocity is $u_{\rm cr} \simeq \sqrt{8p_{\rm st}/5\rho}$.

Note that, for an arbitrary acceleration (assuming $\dot{\mathbf{u}} \| \mathbf{u}$), one can introduce the effective damping rate $\nu_{\rm eff} = \nu + \dot{u}/u$, which can have either sign, so that the critical cosine $\xi_{\rm cr}$ can have either sign as well. Thus, if the projectile experiences a sufficiently strong deceleration ($|\dot{u}|/u > \nu$), the cavity can also be deformed at the front hemisphere.

The critical velocity $u_{\rm cr}$ calculated above defines the emergence of a point or a circle of zero pressure on the cavity surface depending on the value of $\xi_{\rm cr}$. It is well known in the gas dynamics that the existence of small local regions of negative pressure would not lead to a significant deformation of flow lines and, therefore, to a stall. Instead, the emergence of a stall requires an extended region of negative pressure that covers a significant part of the "rear hemisphere". There does not seem to be any criterion that would tell us how large the negative region should be to initiate a stall. Nevertheless, one can hope that the velocity $u_{\rm cr}$ derived above provides a reasonable lower bound estimate for the cavity deformation onset. Strictly speaking, the theory discussed above is not applicable to the case $u > u_{\rm cr}$, because a streamlined cavity is already deformed. At the same time, this deformation is small below the stall threshold, i.e., the cavity is still almost spherical. Therefore, one could extend the analysis to the region of velocities higher than the critical one and, respectively, to the region of negative pressure larger than a point or a circle on the cavity surface. In the next section, the obtained results are generalized to the case of the finite compressibility of a fluid.

4. Flow with Finite Compressibility

In this section, we will estimate the effect of finite compressibility of the dust cloud on the velocity and pressure fields. Here, we will treat a steady ($\dot{\mathbf{u}} = 0$) and irrotational ($\nabla \times \mathbf{v} = 0$) flow, so that the fluid density is a function solely of the radius-vector: $\rho = \rho(\mathbf{r})$. Since $\nabla \times \mathbf{v} = 0$ and $\nabla p = c^2 \nabla\rho$, where $c = \sqrt{(\partial p/\partial\rho)_T}$ is the sound velocity, we can rewrite Eq. (1) in the form

$$(\mathbf{v} \cdot \nabla)\mathbf{v} + \nu(\mathbf{v} + \mathbf{u}) = -\frac{c^2}{\rho}\nabla\rho. \tag{13}$$

In this case, the continuity equation includes the fluid density,

$$\nabla \cdot \mathbf{v} + \mathbf{v} \cdot \frac{\nabla\rho}{\rho} = 0. \tag{14}$$

Here, c is assumed to be constant independent of the local velocity and plasma state parameters. We substitute $\nabla\rho/\rho = -(1/c^2)(\mathbf{v} \cdot \nabla)\mathbf{v} - (\nu/c^2)(\mathbf{v} + \mathbf{u})$ from (13) in (14) to derive

$$\nabla \cdot \mathbf{v} = \frac{1}{c^2}\mathbf{v} \cdot (\mathbf{v} \cdot \nabla)\mathbf{v} + \frac{\nu}{c^2}(v^2 + \mathbf{u} \cdot \mathbf{v}). \tag{15}$$

We will search for a solution of Eq. (15) in the form $\mathbf{v} = \mathbf{v}_0 + \mathbf{v}_1$, where $\mathbf{v}_0(\mathbf{r})$ is a solution of the

incompressible problem (for $\rho = \rho_0 = \text{const}$, i.e., for $c \to \infty$) given by Eq. (5), the respective pressure distribution $p_0(\mathbf{r})$ is presented by Eq. (10) (for $\dot{u} = 0$). Obviously, $\nabla \cdot \mathbf{v}_0 = 0$. We assume that $|\mathbf{v}_1| \ll |\mathbf{v}_0|$ and retain solely zeroth-order terms on the rhs of (15) to obtain

$$\nabla \cdot \mathbf{v}_1 = \frac{1}{2c^2}\mathbf{v}_0 \cdot \nabla v_0^2 + \frac{\nu}{c^2}\left(v_0^2 + \mathbf{u} \cdot \mathbf{v}_0\right). \qquad (16)$$

The solution of Eq. (16) with the boundary conditions $\mathbf{v}_1(\infty) = 0$ and $\mathbf{n} \cdot \mathbf{v}_1 |_{r=R} = 0$ was obtained in [31]. On the cavity surface, it has the form

$$\mathbf{v}_1 |_{r=R} = \frac{u^2}{c^2}\left(\frac{243}{176}\xi^2 + \frac{\kappa}{4}\xi - \frac{551}{880}\right)(\mathbf{u} - \xi u\mathbf{n}). \qquad (17)$$

As it could be expected from symmetry considerations, $\mathbf{v}_1 |_{r=R} = 0$ at $\xi = \pm 1$, i.e, at both poles. Along with Eq. (13), this solution makes it possible to calculate the correction to the pressure distribution over the cavity surface due to the finite compressibility of a dust cloud. If we confine ourselves to the terms proportional to u^2, then we arrive at [31]

$$p(\xi) \simeq p_{\text{st}} + \frac{\rho_0 u \nu R}{2}\xi + \frac{\rho_0 u^2}{8}\left(9\xi^2 - 5 + \frac{4\nu^2 R^2}{3c^2}\right) \qquad (18)$$

instead of (10). Thus, the pressure increases due to the finite compressibility, so that the threshold velocity of a cavity deformation increases as well. On the other hand, one can see that the resulting correction is small when $\kappa u/c \ll 1$. However, we will see that the finite compressibility correction is always small for large projectiles, even if this condition is not satisfied. It is worth mentioning that, even in the general case, the obtained correction to the pressure includes solely even powers of ξ, so that the corresponding correction to an additional force exerted on the projectile due to the dissipation in the surrounding particle fluid (11) vanishes.

Now, we repeat the analysis of Section 3 for Eq. (18) instead of (10). Since the finite compressibility correction is independent of ξ, the expression for ξ_{cr} remains the same as in Section 3. First, we consider the case $|\xi_{\text{cr}}| > 1$. Then we have to set $\xi = -1$ in Eq. (18) to find the threshold velocity corresponding to the emergence of a point of zero pressure at the "rear pole" of a cavity:

$$u_{\text{cr}} = \frac{\nu R}{2\omega} - \sqrt{\frac{\nu^2 R^2}{4\omega^2} - \frac{2p_{\text{st}}}{\omega\rho_0}} \simeq \frac{2p_{\text{st}}}{\nu R \rho_0}, \qquad (19)$$

where $\omega = 1 + \nu^2 R^2/3c^2$. For the case of large cavities ($R \to \infty$) typical of the treated case, approximation (19) is valid provided that the condition $p_{\text{st}}/\rho_0 c^2 \ll 1$, which applies to experiments analyzed in Section 5, is satisfied even if $\kappa u/c > 1$. Thus, the finite compressibility seems to have no significant effect on the critical velocity. The reciprocal dependence $p_{\text{st}}(u_{\text{cr}})$ has the form

$$\frac{p_{\text{st}}}{\rho_0} = \frac{\omega u_{\text{cr}}^2}{2}\left(\frac{\nu R}{\omega u_{\text{cr}}} - 1\right) \simeq \frac{1}{2}\nu R u_{\text{cr}}. \qquad (20)$$

Upon a further increase of the projectile velocity u, the region of negative pressure on the surface of a cavity is expanded. It is a straightforward matter to demonstrate that the extrapolation of the theory to the extended region of negative pressures (where it is formally invalid) results in a very fast increase of this region with the increase of u. Therefore, u_{cr} is likely to be a good estimate for the stall velocity u_{st}. At the same time, $u_{\text{st}} > u_{\text{cr}}$ means that if we equate $u_{\text{cr}} = u_{\text{st}}$, relation (20) yields an overestimated p_{st}, which can be treated as *an upper bound estimate* for the static pressure.

In the case $|\xi_{\text{cr}}| < 1$ typical of small projectiles, a circle with zero pressure firstly emerges at the critical velocity

$$u_{\text{cr}} = 2\left(\frac{2p_{\text{st}}}{5\rho_0} - \frac{\nu^2 R^2}{45}\right)^{1/2} \times$$
$$\times \left(1 - \frac{4\nu^2 R^2}{15c^2}\right)^{-1/2} \simeq \left(\frac{8p_{\text{st}}}{5\rho_0}\right)^{1/2}. \qquad (21)$$

Here, the approximation corresponding to the limit $R \to 0$ also coincides with that for an incompressible fluid. If u_{cr} is known from experiment, one can derive an upper bound estimate for the static pressure,

$$\frac{p_{\text{st}}}{\rho_0} = \frac{5u_{\text{cr}}^2}{8} + \frac{\nu^2 R^2}{18}\left(1 - \frac{3u_{\text{cr}}^2}{c^2}\right) \simeq \frac{5u_{\text{cr}}^2}{8}. \qquad (22)$$

In this case at $u > u_{\text{cr}}$, the circle expands to a region between two circles on the surface of a cavity. For small projectiles, one can also demonstrate that a fast expansion of the negative region takes place as u is increased. Thus, u_{cr} also yields a reasonable order of magnitude for an estimate of the stall threshold.

5. Comparison with Experiment

Based on the developed theory, we will analyze the possibility of a cavity deformation in experiments. First, let us consider the experiments carried

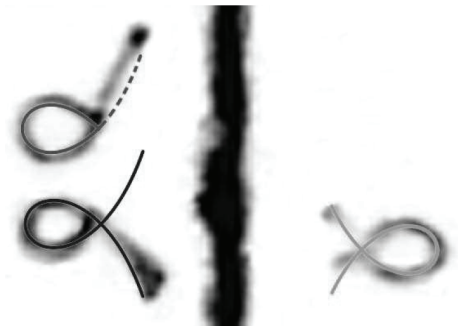

Fig. 5. (Color online) Individual dust particles moving along the α-shaped pathways. Traces are the superposition of frames obtained in the experiment (negative image, vertical trace marks the projectile trajectory), solid lines show the result of calculation by formulas (8) and (9), dashed line indicates the trajectory portion "forced" by the local crystallization

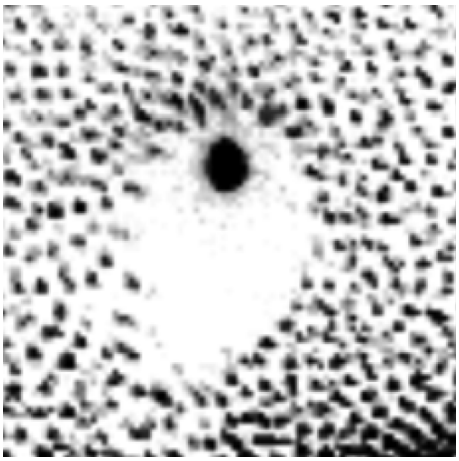

Fig. 6. Deformed cavity around a large subsonic projectile moving with the velocity $u = 1.8$ cm/s. Reproduction of an enlarged fragment of Fig. 3, *a* in Ref. [11]

out in the PK-3 Plus Laboratory on the board of the ISS under microgravity conditions discussed in Section 2.

Figure 5 shows a good correspondence between solution (8), (9) and experimentally observed traces of individual particles in their closed portions obtained by superposition of frames. Indication of this correspondence is a good agreement between the ratio of the height of a closed loop to R determined experimentally (Fig. 5), which amounts to about 0.28, while the theoretical value is 0.277. This ratio is independent of the loop position relative to the projectile path. Note that since the streamline takes place in a close neighborhood of the projectile and farther regions are crystallized, an approximate solution (8), (9) utilizing the same approximation seems to be even more adequate to the treated system than the numerical solution. Open portions of particle traces reveal some differences from theory. In Fig. 5, the upper trace portion of the bottom loop on the left-hand side seems to disappear due to the fact that the particle goes out of the illumination plane. On the contrary, the upper trace portion of the top loop on the left-hand side would not appear at all, but the particle was probably pushed toward the projectile due to a spatial re-distribution of particles in the course of local crystallization. A good correspondence between theory and experiment demonstrates that the stream flow of dust particles is almost a potential nonviscous one.

Consider the onset of the deformation of a cavity around the moving projectile. For a gas pressure of 10 Pa and and the temperature $T_n = 300$ K, respectively, we have $m_n = 6.63 \times 10^{-23}$ g, $n_n = 2.42 \times \times 10^{15}\,\mathrm{cm}^{-3}$, and $v_{T_n} = 2.5 \times 10^4$ cm/s. Under these conditions for dust particles, we have $\nu = 46.6\,\mathrm{s}^{-1}$.

Successive frames of the projectile path recorded by a high-resolution camera are shown in Fig. 3. The projectile velocity increases slowly from $u = 0.7$ cm/s to 1.4 cm/s. Since the sound velocity measured in this experiment amounts to 2.2 cm/s [19], such motion is subsonic. The peculiarity of this motion is an abrupt change of the cavity configuration. At the beginning, the projectile moves in the center of a cavity [cf. Figs. 3, *a* and *b*]. Then, at the point of trajectory characterized by the velocity $u = 1.06$ cm/s, acceleration $\dot{u} = 2.6$ cm/s^2, and the cavity radius $R = 3.74 \times 10^{-2}$ cm, the projectile shifts abruptly from the cavity center to its front side (Fig. 3, *c*). In the course of further motion, the cavity deformation is preserved (Fig. 3, *d*). One can assume that, at the point shown in Fig. 3,*c*, the velocity of the accelerating projectile exceeds the stall threshold. Under specified experimental conditions, $\xi_{\mathrm{cr}} = -0.365$; hence, we substitute $u_{\mathrm{cr}} = 1.06$ cm/s in (22) to derive an upper bound estimate $p_{\mathrm{st}}/\rho_0 \approx 0.753$ cm^2/s^2 (or $p_{\mathrm{st}} \approx 3.0 \times 10^{-7}$ Pa). Note that the correction for the acceleration to the total pressure $-\rho\dot{u}R/2$ [Eq. (10)] is small due to a small projectile acceleration at the selected point ($\dot{u}/u \ll \nu$) and can be neglected.

The estimate obtained above can be compared with a theoretical estimation for the static pressure, which

is based on dimensionality considerations. Since the dimensionalities of the pressure and the energy density coincide, we can write $p_{\rm st} \sim Z_{\rm d}^2 e^2 n_{\rm d}/2\bar{r}$ with an order-of-magnitude accuracy, where $\bar{r} = (3/4\pi n_{\rm d})^{1/3}$ is the Wigner–Seitz radius for a dust crystal, and $n_{\rm d}$ is the number density of dust particles. With $Z_{\rm d} = 1200$ and $n_{\rm d} = 3 \times 10^5$ cm^{-3} [19], this estimation yields $p_{\rm st} \sim 5.4 \times 10^{-7}$ Pa, which correlates with the upper bound estimate resulting from experiment.

Microgravity conditions can also be maintained on parabolic flights. Such experiments were performed using the IMPF-K2 chamber [11]. The experiment was carried out with argon at 30 Pa and $a_{\rm d} = 4.775 \times 10^{-4}$ cm ($M_{\rm d} = 6.88 \times 10^{-10}$ g and $\nu = 33.5$ s^{-1}). Projectiles were accelerated by a special device (cogwheel) up to both supersonic and subsonic velocities. A typical image illustrating the motion of a subsonic projectile inside a dust cloud is shown in Fig. 6. Both the projectile shift from the cavity center toward its front side and the nonspherical (elongated) shape of a cavity are visible. Unfortunately, a point of transition from a spherical to a deformed cavity was not detected in this experiment. Nevertheless, we can estimate the stall threshold for this case. Note that the estimate $p_{\rm st} \sim Z_{\rm d}^2 e^2 n_{\rm d}/2\bar{r}$ with $Z_{\rm d} = 8800$ and $n_{\rm d} = 2 \times 10^4$ cm^{-3} [11] yields $p_{\rm st} \sim 7.8 \times 10^{-7}$ Pa, which is close to the estimate for experiment [22] discussed above. Therefore, we can assume that $p_{\rm st}$ are close in both systems and use the upper bound estimate (19) to calculate $u_{\rm cr}$ for the treated system. With the cavity radius roughly estimated as $R = 0.1$ cm, we derive $u_{\rm cr} \approx 0.462$ cm/s, so that the projectile moves in the low-velocity regime ($\xi_{\rm cr} = -1.61$). Therefore, the stall threshold for this system does not exceed 1 cm/s. This result correlates with the projectile velocity in Fig. 6, $u = 1.8$ cm/s, which is still lower than the sound velocity $c = 2.0$ cm/s [11]. Thus, the main notion of the present study, namely that the cavity around a moving projectile can be deformed at *subsonic velocity*, is corroborated.

6. Conclusion

In this study, we have observed that a projectile going through the dust crystal with a subsonic velocity appears to move almost freely. We have proposed a new explanation of this fact implying a nonviscous flow of dust particles about the projectile, in which the interaction force between the projectile and dust particles vanishes. To prove this, we monitored the particle dynamics by means of a high-resolution camera. Superposition of successive frames revealed typical α-shaped pathways of dust particles in the neighborhood of projectile. Since the system is strongly coupled, it can be divided into the Wigner–Seitz cells around each particle including the projectile, whose motion does not break a close ordering. However, the projectile melts the crystal in its neighborhood, and the dust particles flow about the projectile cell boundary in such a way that the distance R between individual dust particles and the projectile, which can be measured using recorded frames, is the sum of radii of the Wigner–Seitz cells around dust particles and the projectile. In the framework of our model, we have to imply that the cells around particles rather than the particles themselves take part in the interaction. In the absence of direct interparticle contacts, the shear viscosity must vanish, and we can consider the nonviscous flow of cells.

The classical solution for the velocity field in a potential nonviscous flow about a sphere moving with a constant velocity can be regarded as a system of differential equations for the trajectories of individual dust particles. We have solved these equations numerically and obtained an analytical solution, which approximates closely the numerical one. This solution, which defines the coordinates of dust particles as explicit functions of the time, is in a good agreement with particle trajectories obtained experimentally by a superposition of successive frames. Thus, the motion of a projectile implies no momentum transfer from the liquid to the projectile, the drag force arising from the interaction between the projectile and dust particles must *vanish*, i.e., a large particle can move almost freely inside the bulk of a strongly coupled dust crystal. Our investigation also points to the fact that the hydrodynamic approach can be valid at small length scales down to several interparticle distances.

In addition, we have investigated the possibility of a deformation of the cavity around a large projectile slowly moving inside a cloud of small dust particles. This cavity is formed due to a strong Coulomb repulsion between the projectile and dust particles. Since the parameter $\beta_{\rm dp}$ characterizing this interaction is very large, the cavity deformation occurs solely due to the formation of a void adjacent to the initially spherical cavity. This is similar to the process of void formation in a fluid under negative

pressure. Since we approximate the dust cloud by a system of hard spheres, zero pressure is sufficient for the void formation leading to a cavity deformation.

We model the collective particle subsonic motion in a complex plasma by a nonviscous irrotational hydrodynamic motion of the dust fluid and show that, in this model, the reason for the cavity deformation is the friction between dust particles and neutral atoms of a carrier gas. It is this friction that stipulates the emergence of a zone of negative pressure over the back of the cavity surface. If such a zone covers a substantial part of the surface, the stall takes place, which is observed as a cavity deformation. We have found that the deformation is more likely to be observed for larger projectiles. The deformation occurs when the projectile velocity exceeds some threshold of a subsonic velocity.

Since the typical projectile velocities are of the same order of magnitude as the sound velocity, we have studied the effect of a finite compressibility of the dust fluid on the velocity and pressure fields. Toward that end, we have obtained an exact solution of the linearized gas dynamics equations for a compressible nonviscous fluid flowing about the cavity. In so doing, we included both the convective and friction terms in the Navier–Stokes equation. Calculations showed that the corrections for a finite compressibility are rather small. Generally, the account of the compressibility leads to a shift of the area covered by a negative pressure zone.

The analysis of available experimental data has validated our approach. It was found that the cavity is deformed when either the velocity [22] or the size [11] of a projectile is sufficiently large. It is worth mentioning that the phenomenon of cavity deformation is similar to the formation of a void behind a cluster of smaller particles moving in the cloud of larger ones [32]. For intermediate projectile sizes, a transition from a spherical to a deformed cavity was observed along the trajectory of an individual projectile. The transition threshold is in accordance with the developed theory. This made it possible to estimate the static pressure inside a dust cloud and, hence, opened up a possibility to use projectiles as a diagnostic tool for the dust equation of state.

1. *Complex and Dusty Plasmas: from Laboratory to Space*, edited by V.E. Fortov and G.E. Morfill (CRC Press, Boca Raton, 2009).
2. J.H. Chu and I. Lin, Phys. Rev. Lett. **72**, 4009 (1994).
3. H. Thomas, G.E. Morfill, V. Demmel, J.Goree, B. Feuerbacher, and D. Möhlmann, Phys. Rev. Lett. **73**, 652 (1994).
4. Y. Hayashi and S. Tashibana, Jpn. J. Appl. Phys. **33**, L804 (1994).
5. S.V. Vladimirov, K. Ostrikov, and A.A. Samarian, *Physics and Applications of Complex Plasmas* (Imperial College, London, 2005).
6. V. Fortov, A. Ivlev, S. Khrapak, A. Khrapak, and G. Morfill, Phys. Rep. **421**, 1 (2005).
7. G.E. Morfill and A.V. Ivlev, Rev. Mod. Phys. **81**, 1353 (2009).
8. P.K. Shukla and B. Eliasson, Rev. Mod. Phys. **81**, 25 (2009).
9. M. Bonitz, C. Henning, and D. Block, Rep. Prog. Phys. **73**, 066501 (2010).
10. G.E. Morfill, U. Konopka, M. Kretschmer, M. Rubin-Zuzic, H.M. Thomas, S.K. Zhdanov, and V. Tsytovich, New J. Phys. **8**, 7 (2006).
11. D. Caliebe, O. Arp, and A. Piel, Phys. of Plasmas **18**, 073702 (2011).
12. A. Piel, O. Arp, M. Klindworth, and A. Melzer, Phys. Rev. E **77**, 026407 (2008).
13. K.O. Menzel, O. Arp, and A. Piel, Phys. Rev. E **83**, 016402 (2011).
14. O. Arp, D. Caliebe, and A. Piel, Phys. Rev. E **83**, 066404 (2011).
15. M. Schwabe, S.K. Zhdanov, H.M. Thomas, A.V. Ivlev, M. Rubin-Zuzic, G.E.Morfill, V.I. Molotkov, A.M. Lipaev, V.E. Fortov, and T. Reiter, New J. Phys. **10**, 033037 (2008).
16. G.E. Morfill, H.M. Thomas, U. Konopka, H. Rothermel, M. Zuzic, A. Ivlev, and J. Goree, Phys. Rev. Lett. **83**, 1598 (1999).
17. S.A. Khrapak, B.A. Klumov, P. Huber, V.I. Molotkov, A.M. Lipaev, V.N. Naumkin, H.M. Thomas, A.V. Ivlev, G.E. Morfill, O.F. Petrov *et al.*, Phys. Rev. Lett. **106**, 205001 (2011).
18. H.M. Thomas, G.E. Morfill, V.E. Fortov, A.V. Ivlev, V.I. Molotkov, A.M. Lipaev, T. Hagl, H. Rothermel, S.A. Khrapak, R.K. Suetterlin *et al.*., New J. Phys. **10**, 033036 (2008).
19. M. Schwabe, K. Jiang, S. Zhdanov, T. Hagl, P. Huber, A.V. Ivlev, A.M. Lipaev, V.I. Molotkov, V.N. Naumkin, K.R. Süutterlin *et al.*., EPL **96**, 55001 (2011).
20. M.-C. Chang, Y.-P. Tseng, and I. Lin, Phys. of Plasmas **18**, 033704 (2011).
21. D. Samsonov, J. Goree, H.M. Thomas, and G.E. Morfill, Phys. Rev. E **61**, 5557 (2000).
22. D.I. Zhukhovitskii, V.E. Fortov, V.I. Molotkov, A.M. Lipaev, V.N. Naumkin, H.M. Thomas, A.V. Ivlev, M. Schwabe, and G.E. Morfill, Phys. Rev. E **86**, 016401 (2012).
23. A.V. Ivlev and D.I. Zhukhovitskii, Phys. Plasmas **19**, 093703 (2012).
24. V.E. Fortov, O.F. Petrov, A.D. Usachev, and A.V. Zobnin, Phys. Rev. E **70**, 046415 (2004).

25. J. Goree, G.E. Morfill, V.N. Tsytovich, and S.V. Vladimirov, Phys. Rev. E **59**, 7055 (1999).
26. V. Nosenko, A.V. Ivlev, and G.E. Morfill, Phys. Plasmas **17**, 123705 (2010).
27. V.A. Schweigert, I.V. Schweigert, V. Nosenko, and J. Goree, Phys. Plasmas **9**, 4465 (2002).
28. B. Liu, J. Goree, V. Nosenko, and L. Boufendi, Phys. Plasmas **10**, 9 (2003).
29. B. Buttenschön, M. Himpel, and A. Melzer, New J. Phys. **13**, 023042 (2011).
30. L.D. Landau and E.M. Lifshitz, *Fluid Mechanics* (Pergamon Press, New York, 1959).
31. D.I. Zhukhovitskii, A.V. Ivlev, V.E. Fortov, and G.E. Morfill, Phys. Rev. E **87**, 063108 (2013).
32. K.R. Sütterlin, A. Wysocki, A.V. Ivlev, C. Räth, H.M. Thomas, M. Rubin-Zuzic, W.J. Goedheer, V.E. Fortov, A.M. Lipaev, V.I. Molotkov *et al.*., Phys. Rev. Lett. **102**, 085003 (2009).

Received 28.11.13

Д.І. Жуховицький, В.Є. Фортов,
В.І. Молотков, А.М. Липаєв, В.Н. Наумкін,
Х.М. Томас, А.В. Івлєв, Г.Е. Морфіл

ДОЗВУКОВИЙ РУХ ЧАСТИНКИ
В РІДИНІ КОМПЛЕКСНОЇ ПЛАЗМИ
В УМОВАХ МІКРОГРАВІТАЦІЇ

Р е з ю м е

За допомогою лабораторії РК- 3 Plus на борту Міжнародної космічної станції проведені дослідження дозвукового руху великої частинки через об'єм плазмового кристала, який утворюється негативно зарядженими дрібними частинками. Вивчення траєкторії частинок показує, що більша частинка рухається майже вільно через обсяг плазмового кристала, в той час як частинка пилу описує α-образні траєкторії поруч. Розробляється теорія нев'язкого руху частинок для розрахунку їх траєкторій. Досліджена деформація порожнини навколо великої частинки, що рухається з дозвуковою швидкістю в хмарі дрібних частинок пилу з урахуванням тертя між частинками пилу і атомів нейтрального газу. Тиск пилової хмари на поверхні порожнини навколо великої частинки може стати негативним, що тягне за собою появу значної асиметрії порожнини, тобто її деформації. Результати розрахунків погоджуються з експериментальними даними.

Д.И. Жуховицкий, В.Е. Фортов,
В.И. Молотков, А.М. Липаев, В.Н. Наумкин,
Х.М. Томас, А.В. Ивлев, Г.Е. Морфил

ДОЗВУКОВОЕ ДВИЖЕНИЕ ЧАСТИЦЫ
В ЖИДКОСТИ КОМПЛЕКСНОЙ ПЛАЗМЫ
В УСЛОВИЯХ МИКРОГРАВИТАЦИИ

Р е з ю м е

С помощью лаборатории РК-3 Plus на борту Международной космической станции проведены исследования дозвукового движения большой частицы через объем плазменного кристалла, который образуется отрицательно заряженными мелкими частицами. Изучение траектории частиц показывает, что большая частица движется почти свободно через объем плазменного кристалла, в то время как частица пыли описывает α-образные траектории рядом. Разрабатывается теория невязкого движения частиц для расчета их траекторий. Исследована деформация полости вокруг большой частицы, движущейся с дозвуковой скоростью в облаке мелких частиц пыли с учетом трения между частицами пыли и атомов нейтрального газа. Давление пылевого облака на поверхности полости вокруг большой частицы может стать отрицательным, что влечет за собой появление значительной асимметрии полости, то есть ее деформации. Результаты расчетов согласуются с экспериментальными данными.